Design of a Dual-port, Side-incident Microwave Probe for Detection of In-Pipe Damage

doi: 10.1088/1361-6501/ab9acc

Design of a Dual-port, Side-incident Microwave Probe for Detection of In-Pipe Damage

Guanren Chen*, Takuya Katagiri, Noritaka Yusa, Hidetoshi Hashizume

Department of Quantum Science and Energy Engineering, Graduate School of Engineering, Tohoku University, 6-6-01-2, Aramaki Aza Aoba, Aoba, Sendai, Miyagi 980-8579, Japan

Abstract

This study reports a dual-port, side-incident microwave probe dedicated to the non-destructive inspection of metal pipes. Two types of side-incident probes (LJ and JL) are proposed to emit TM_{01} and TM_{02} mode microwaves into the pipe under test, and each type of probe has two ports used to inspect two opposite directions. Numerical simulations are conducted to study the dimensional parameters affecting the transmission characteristic of the probe and optimize the probe to obtain better mode purity and transmission directivity. The simulation results also suggest that the optimal probe dimensions for one inner pipe diameter can be applied to another diameter by multiplying the dimensions by a factor that is determined by the ratio of two diameters. Two LJ-type, side-incident probes with an inner diameter of 19 mm or 39 mm are fabricated according to the simulation results. The experimental verification is subsequently carried out to test the detection directivity of the probes by detecting the short pipes with partially milled damage situated on both sides of each probe. Experimental results show that the proposed dual-port, side-incident probe can effectively detect the in-pipe damage on either side of the probe using the corresponding port and thus realize the directional pipe inspection. Furthermore, this method shows a prospect of being applied to various inner pipe diameters.

Keywords: electromagnetic non-destructive inspection, side-incident, in-pipe damage, mode converter

1. Introduction

Pipelines are an efficient and economical approach for substance transportation, and they are widely employed in a variety of industrial facilities. Metal pipes in pipelines or piping systems may face the problem of failure, which can be caused by fatigue, stress, and corrosion. Therefore, the periodical inspection and maintenance of pipes has become increasingly necessary. Some non-destructive testing (NDT) methods, such as ultrasonic testing [1,2] and eddy current testing [3,4], have been developed and adopted for pipe inspection. However, although these methods have a high detection accuracy, they also require surface preparations or probe scans, which reduce the inspection efficiency and limit their usage for large-scale pipe inspection.

To realize a rapid and long-range pipe inspection, an NDT technology using microwaves has been proposed [5,6]. The principle of this method is interpreted as follows: microwaves of specific mode(s) are emitted into a metal pipe as guided waves and propagated inside the pipe at a speed close to light speed. As the energy of the microwaves is mostly confined inside the pipe, the attenuation is small and thus a long-distance transmission can be achieved. If there is a flaw on the inner surface of the pipe, the propagation of the microwaves will be disrupted, and an echo will be generated. Therefore, the flaw can be detected and located by measuring the reflection and analyzing the time-domain signal. Previous studies have proved that this method could effectively detect multiple types of flaws, such as

pipe wall thinning [7,8], cracks [9-11], and corrosion under insulator [12]. A detection range of 26.5 m has been identified, and the application of this method to bent pipe inspection has been examined [14,15].

Most previous studies on microwave NDT focused on exciting microwaves from the pipe end. However, the pipe end may not be open for probe insertion in some complicated piping systems. A single-port, side-incident microwave probe [16] was proposed to resolve this problem. The structure of the probe is shown in figure 1 (a). The TEM mode microwaves are emitted into the pipe under test from the pipe sidewall through a bent semi-rigid coaxial cable inserted into the pipe. The direction of the propagation of the microwaves inside the pipe can be altered by specifically selecting the frequency range as shown in figures 1 (b) and (c). When the frequency ranges from 18.5 GHz to 25.5 GHz, the TM_{01} mode microwaves mainly propagate inside the pipe to the right direction; when the frequency ranges from 30 GHz to 37 GHz, the TM_{02} mode microwaves mainly propagate inside the pipe to the left direction. However, as only a limited number of numerical simulations were performed in the previous study, the dimensional parameters influencing the transmission characteristic of the probe were not completely clarified. Thus, the probe was not adequately optimized to obtain better mode purity and transmission directivity. For example, as highlighted by the black arrow in figure 1(b), a portion of the TM_{01} mode microwaves (mainly transmitted to the right) is also transmitted to the left side, and this could lead to a misjudgment or interference in analyzing the reflection signals. Moreover, in the previous study, only the probe with an inner diameter of 19 mm was studied and developed, while the viability of applying this side-incident method to other diameters was not discussed.

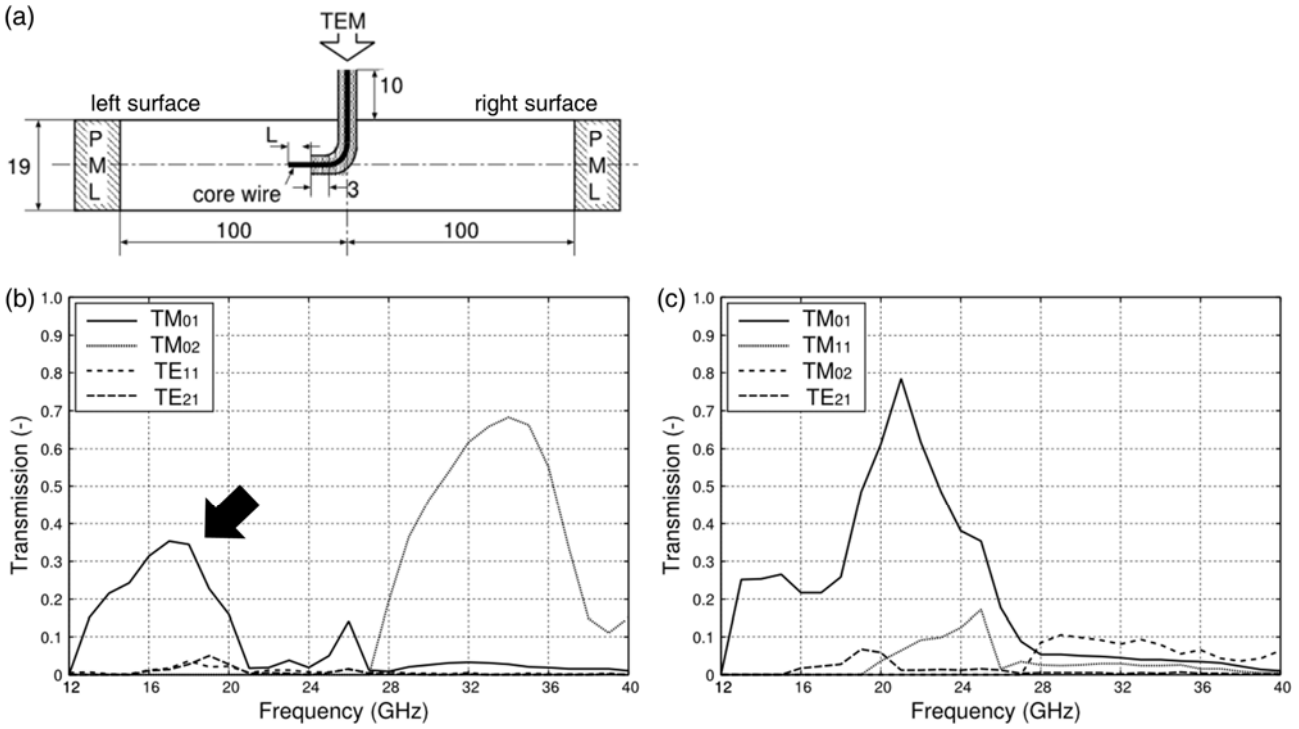

Figure 1. Single-port, side-incident microwave probe, (a) structure, (b) microwave modes transmitted to the left surface, and (c) microwave modes transmitted to the right surface.[16]

In an attempt to address the issues mentioned above, this study proposes a dual-port, side-incident microwave probe that can realize the directional dual-way pipe inspection. The rest of this manuscript is organized as follows. In Section 2, numerical simulations are carried out to investigate the

dimensional parameters influencing the transmission characteristics of the probe, and two types of dual-port, side-incident probes are proposed and optimized to acquire good mode purity and transmission directivity. In Section 3, experimental verification is conducted to confirm the effectiveness of the probe in specifically detecting flaws at different positions in pipes, and the applicability of this method to other inner pipe diameters is validated. The conclusions are presented in Section 4. Some supplementary information is given in the appendix.

2. Numerical simulation

In this section, three-dimensional numerical simulations are carried out for both the previous single-port probe and the newly proposed dual-port probe. The single-port probe is simulated to investigate the dimensions affecting the transmission characteristic of the probe and to obtain an optimized result for the single-way microwave transmission. The simulation for the dual-port probe is conducted based on the results of the single-port probe simulation to evaluate the mode purity and transmission directivity of the proposed dual-port model in two directions. The feasibility of applying the side-incident method to other pipe diameters is also discussed.

2.1 Simulation environment

A commercial finite element simulation software COMSOL Multiphysics v5.2a with the RF module was applied for computation. The electric field was solved three-dimensionally in the frequency domain. The governing equation is given below:

$$\nabla \times \mu_{\mathrm{r}}^{-1}(\nabla \times \boldsymbol{E}) - k_0^2[\varepsilon_{\mathrm{r}} - \mathrm{j}\sigma/(\omega\varepsilon_0)]\boldsymbol{E} = 0, \quad (1)$$

where $k_0 = \omega\sqrt{\varepsilon_0\mu_0}$ is the propagation constant in a vacuum, ε_0 and μ_0 are the permittivity and permeability in a vacuum, ω is the angular frequency, and j is the imaginary unit. Vector $\boldsymbol{E}$ denotes the electric field, and σ is the electrical conductivity. The parameters ε_{r} and μ_{r} are the relative permittivity and relative permeability, respectively. In this computation, the values are μ_{r} =1, ε_{r} = 1, and σ = 0 for the media air.

2.2 Simulation model and results

2.2.1 Single-port, side-incident probe

The geometrical model of the single-port side-incident shown in figure 2 is basically the same as the model in figure 1 (a), which comprises a cylindrical air entity as the interior of the pipe and a side-inserted semi-rigid coaxial cable. The diameter of the cable core wire was 0.8 mm, and the inner and outer diameters of the outer layer of the cable were 2.2 mm and 2.9 mm [17], respectively. An insulator was filled between the core wire and the outer layer of the cable, and its relative permittivity was 1.687. The inner diameter of the pipe was set to 19 mm, and the perfectly matched layer (PML) was positioned at each end of the pipe to simulate the infinite space. The boundary conditions of the pipe wall and the surface of the cable were defined as the perfect electric conductor. The TEM mode microwaves were excited at the port outside the pipe, and the converted microwaves were transmitted to two directions in the pipe. Two virtual surfaces, which did not interact with electromagnetic fields, were situated at the left side and the right side of the model, 100 mm relative to the inserted cable. The two surfaces were defined as the left surface and right surface, highlighted with the blue and red color in the figure, respectively. The domain-backed slit condition was applied to these two surfaces, and the transmission

characteristic of each mode (S-parameter 21) was evaluated on both left and right surfaces. More specifically, the energy ratio of each mode was evaluated by normalizing the transmitted energy with the input energy of TEM mode. The labels (1) and (2) in the figure denote the ports 1 and 2 for evaluating S-parameter 21, respectively. Some dimensional parameters of the probe were chosen and altered in the simulation to investigate their effects on the transmission characteristic of the probe, including the curvature radius of the bent cable r_C, the exposed length of the cable core wire l_E, the straight portion cable length l_S, and the outer cable length l_V. Table 1 summarizes the values of the investigated parameters in the numerical simulation. The sweeping frequency span f ranged from 12 GHz to 43 GHz, with a step of 0.5 GHz. Second-order tetrahedral and triangular elements were used for discretization.

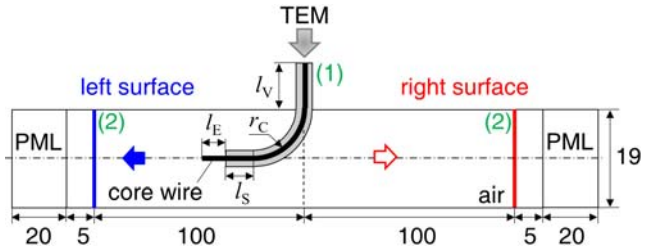

Figure 2. Geometrical model of the single-port, side-incident probe for simulation (unit: mm, not to scale).

Table 1. Simulation parameters of the single-port, side-incident probe

Parameter	r_C	l_E	l_S	l_V*
Value (mm)	4, 5, 6, 7, 8	3, 4, 5	1, 2, 3, 4, 5, 6, 7, 8	10, 20, 30

(*: The parameter l_V was tested just for several groups of r_C, l_E, and l_S. The result of each group indicates that l_V nearly has no influence on the transmission characteristic of the probe as long as the other three parameters are certain.)

A series of simulations were conducted in terms of the parameters listed in Table 1. After analyzing the simulation results of the different parameter combinations, we found that the dimensional parameters r_C, l_E, and l_S jointly affected the transmission characteristic of the probe and that l_V nearly had no influence. The simulation results also suggested that a very good single-way transmission characteristic could be achieved for the TM_{01} or TM_{02} mode microwaves when the aforementioned three key parameters were selected to certain value combinations. As shown in figure 3 (a), when r_C = 7 mm, l_E = 3 mm, and l_S = 8 mm and the frequency ranged from 20.5 GHz to 27.0 GHz, the TM_{01} mode was dominant and mainly transmitted to the right side, the energy ratio of the TM_{01} mode was larger than 0.5, and the energy ratios of the other converted modes were less than 0.1. As shown in figure 3 (b), when r_C = 5 mm, l_E = 5 mm, and l_S = 1 mm and the frequency ranged from 29.5 GHz to 36.5 GHz, the TM_{02} mode was preponderant and basically transmitted to the left side, the energy ratio of the TM_{02} mode was greater than 0.5, and the energy ratios of the other modes were below 0.05. Owing to the space limitation, this section only presents the simulation results of the optimized dimensions (figure 3), which are crucial for the probe design in the following context. The simulation results showing the influence of parameters r_C, l_E, l_S, and l_V are supplemented in the appendix. Compared with the probe in the previous study (figure 1), which can realize the dual-way microwave

propagation with a single port by specifically selecting the span of sweeping frequency, the optimized single-port probe in this section can only implement a single-way transmission but possesses higher mode purity and better transmission directivity. To achieve the dual-way pipe inspection, two ports (cables) should be integrated in the current probe for transmitting microwaves to two opposite directions.

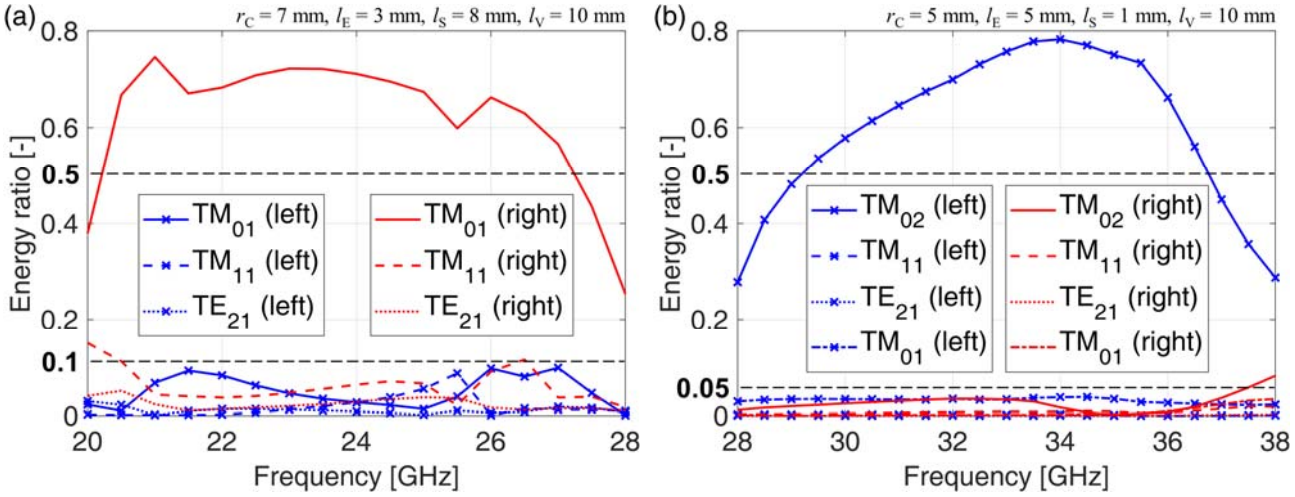

Figure 3. Transmission characteristics of the optimized probes for propagating (a) TM_{01}, (b) TM_{02} mode microwaves.

2.2.2 Dual-port, side-incident probe

On the basis of the results in 2.2.1, we proposed two types of dual-port, side-incident probes: the LJ type and the JL type. The geometric models of the LJ and JL-type probes are illustrated in figure 4 (a) and (b), respectively. Each type of probe had two ports (L and R) for the microwave transmission to the left and right sides, respectively. The dimensions (r_C, l_E, and l_S) of each inserted cable were identical to the optimized results in 2.2.1, and the value of l_V was set to 10 mm. The sweeping frequency step was changed to 0.2 GHz. The S-parameter 21 was evaluated on both left and right surfaces, while the labels (1) and (2) in figure 4 refer to the ports 1 and 2, respectively. The LJ-type probe consisted of two bent cables that were deployed face-to-face as shown in figure 4 (a), and the TM_{01} mode was the dominant mode. The simulation result of the LJ-type, side-incident probe is presented in figure 5, which shows the transmission characteristics when r_C = 7 mm, l_E = 3 mm, l_S = 8 mm, and the TEM mode microwaves were excited at the two ports, respectively. Over the frequency span of 20.6–25.6 GHz, the energy ratio of the TM_{01} mode to either left or right direction was larger than 0.5 and that of the other modes was mostly smaller than 0.1. Clearly, ports L and R were identical as the transmission characteristics of the two ports were consistent, as shown in figure 5 (a) and (b), respectively.

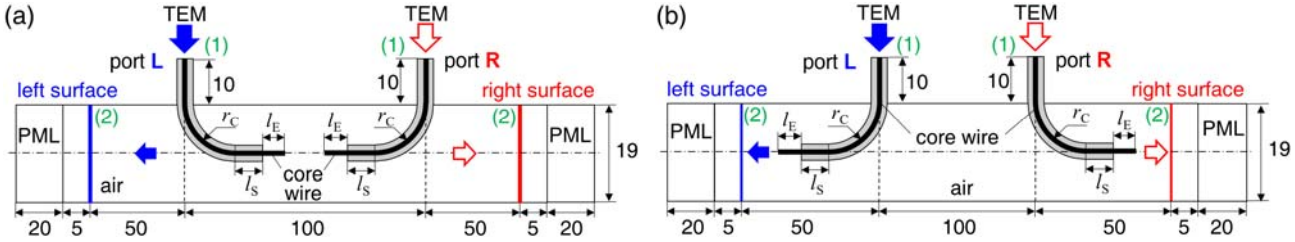

Figure 4. Structures of the dual-port, side-incident probes: (a) LJ type and (b) JL type. (unit: mm, not to scale)

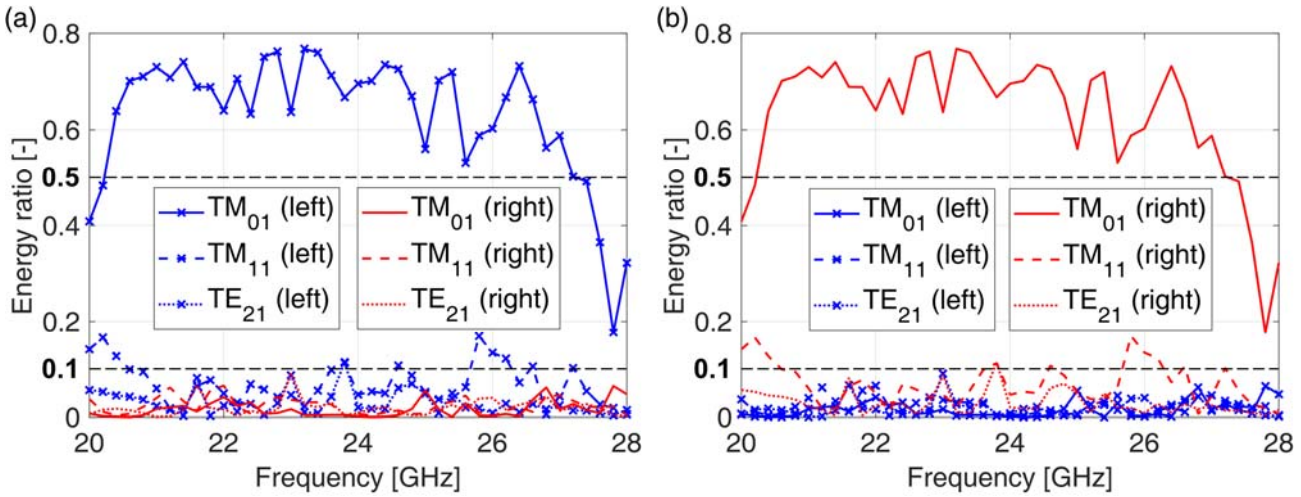

Figure 5. Transmission characteristics of the LJ-type, side-incident probe when r_C = 7 mm, l_E = 3 mm, and l_S =8 mm, (a) port L (b) port R was used.

Similarly, when the inserted cables were deployed back-to-back as shown in figure 4 (b), the TM_{02} mode microwaves were mainly generated, and this type of probe was the JL type. As shown in figure 6, when r_C = 5 mm, l_E = 5 mm, and l_S = 1 mm and the frequency ranged from 29.0 GHz to 36.8 GHz, the fractional energy of the TM_{02} mode was above 0.5 and that of the others was basically below 0.05. The JL-type probe seems to have a better mode purity than the LJ-type probe. However, its relatively higher operating frequency also leads to a quicker signal decay, and bending the cable into smaller curvature radii is difficult. Therefore, in this study, the LJ-type probe was mainly studied and experimentally examined in Section 3. Besides, we also confirmed the distance between the two ports affected the transmission characteristic of the probe. Specifically, a too large or a too small interval could lead to the degradation of mode purity and transmission directivity. Some correlated simulation results are exhibited in the appendix. In this study, the distance between the two ports was set to 100 mm. More effort should be made in future studies to further optimize the transmission characteristic of the proposed probe. In comparison with the results acquired using the single-port probe in 2.2.1, those of the dual-port probes were slightly fluctuant probably because of the interference of the unused port.

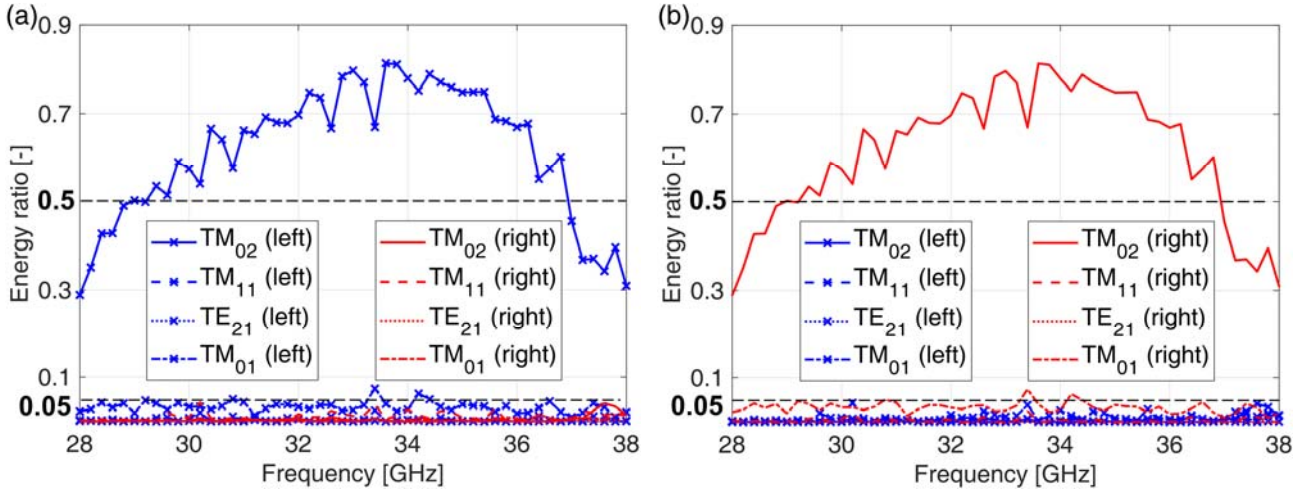

Figure 6. Transmission characteristics of the JL-type, side-incident probe when r_C = 5 mm, l_E = 5 mm, and l_S =1 mm, (a) port L, (b) port R was used.

2.3 Applicability to other inner pipe diameters

The simulation results in 2.2 are valid only on the condition that the inner pipe diameter D is 19 mm. If D is changed to another value, the values of r_C, l_E, and l_S also need to be changed accordingly, which requires additional work for the probe design and optimization.

Hopefully, we have discovered a proportional relationship between the optimized values of r_C, l_E, l_S, and the diameter D, which could significantly reduce time and work for the probe design. For instance, when D is 19 mm, the optimal values of r_C, l_E, and l_S for the LJ-type probe are 7, 3, and 8 mm, respectively. If D is changed to 39 mm, which is about two times of 19 mm, we can simply multiply the optimal values for D =19 mm by a factor 2 as the fiducial values (i.e., 14, 6, and 16 mm) and then make small adjustments to the fiducial values to obtain better performance.

Figure 7 shows the simulation result of the optimized LJ-type probe with D = 39 mm based on the proportional relationship between D and the dimensional parameters. Here, the values of r_C, l_E, and l_S are 14, 7, and 16 mm, respectively. The simulation result shows that, when the frequency span was 8.8–11.6 GHz, the energy ratio of the TM_{01} mode was larger than 0.5, whilst that of the other modes was smaller than 0.1 for both ports L and R. Similarly, if D is changed to 57.5 mm, meanwhile r_C = 21 mm, l_E = 11 mm, l_S = 24 mm, and over the frequency span of 5.7 – 7.3 GHz, the energy ratio of TM_{01} mode is larger than 0.5, while those of other modes are basically below 0.1, as shown in figure 8. These results reveal the potential that the optimized values could be applicable and adaptable to another inner pipe diameter by multiplying the current optimal values by a factor determined by the diameters and making small adjustments to the adapted values.

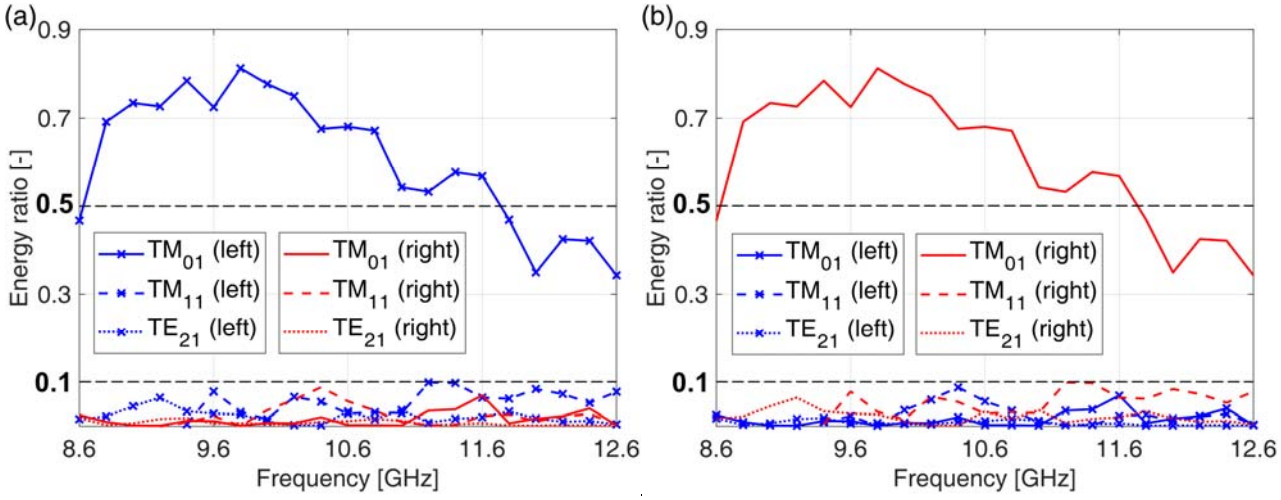

Figure 7. Transmission characteristics of the LJ-type, side-incident probe when D is changed to 39 mm, and r_C = 14 mm, l_E = 7 mm, l_S =16 mm, (a) port L, (b) port R was used.

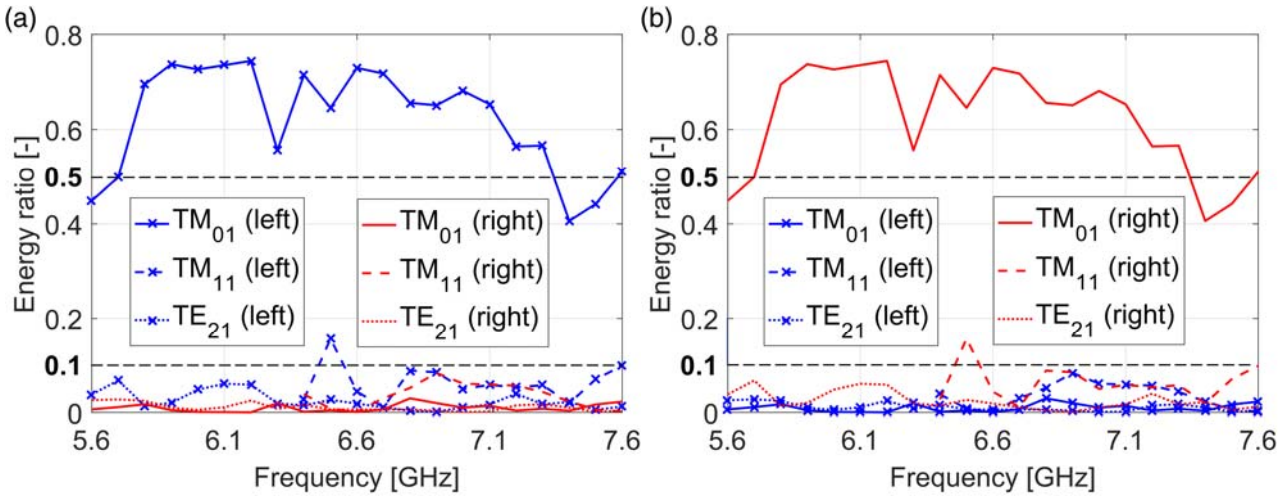

Figure 8. Transmission characteristics of the LJ-type, side-incident probe when D is changed to 57.5 mm, and r_C = 21 mm, l_E = 11 mm, l_S =24 mm, (a) port L, (b) port R was used. (Distance between the two ports was 150 mm)

3. Experiment

Two LJ-type, dual-port side-incident probes with an inner diameter of 19 mm or 39 mm were fabricated in terms of the simulation results in Section 2. An experimental study was conducted to verify the detection directivity of the LJ-type, side-incident probes by detecting the in-pipe damage positioned at different positions in pipes.

3.1 Experimental setup

Figure 9 illustrates an overview of the experimental setup. A network analyzer (not shown in the figure, Agilent Technologies, E8363B) was utilized for generating coaxial TEM mode microwaves after a two-port calibration. The output of the network analyzer was connected to one port (port L or R) of the dual-port, side-incident probe by a flexible coaxial cable (Junkosha, MWX051). The generated TEM mode microwaves were propagated through the flexible cable and subsequently entered the brass pipe (D = 19 or 39 mm) through the side-incident probe, which was deployed at the middle of the pipes under test. Note that only one port worked at one time: when the left pipe was inspected, port L should be connected and port R should be disconnected, and vice versa. The left or right pipe was composed of several 1 m or 1.5 m straight brass pipes connected with flange fittings, and the total length of each pipe was 4 m or 4.5 m. Note that the length of the left pipe and that of the right pipe were different, so that the reflection from any pipe end could be distinguished and determined. Concretely, when port L was connected to inspect the left pipe, the length of the left pipe was 4 m and that of the right pipe was 4.5 m; when port R was connected to inspect the right pipe, the right pipe was 4 m in length and the left pipe was 4.5 m. In brief, the pipe (left or right) that was 4 m in length always corresponded to the port (L or R) in use, and a large reflection peak should be observed at 4 m whereas little reflection should be seen at 4.5 m. To simulate in-pipe damage as a flaw, short pipes with partially milled damage were used in the experiment and situated at different positions in the pipes (points A, B, A', and B') to test the detection directivity of the probe. The detailed configuration of the short pipe is illustrated in Figure 10, and the dimensional parameters of the short pipes are itemized in Table 2. The short pipes Nos. 1 and 4, with no milled damage were used as reference. The original pipe wall thickness for either D = 19 mm or D = 39 mm pipe was 3 mm, and the short pipes were all 50 mm in length. Figure 11 displays the photograph of the experimental setup.

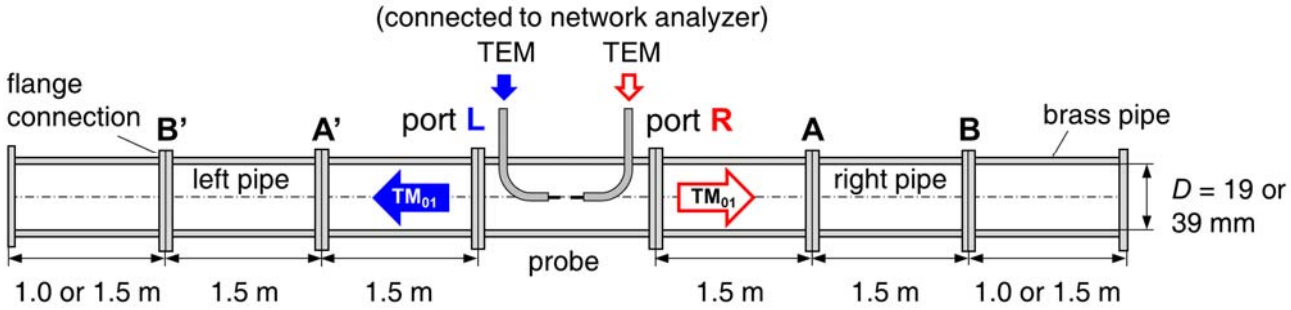

Figure 9. Illustration of the experimental setup (not to scale).

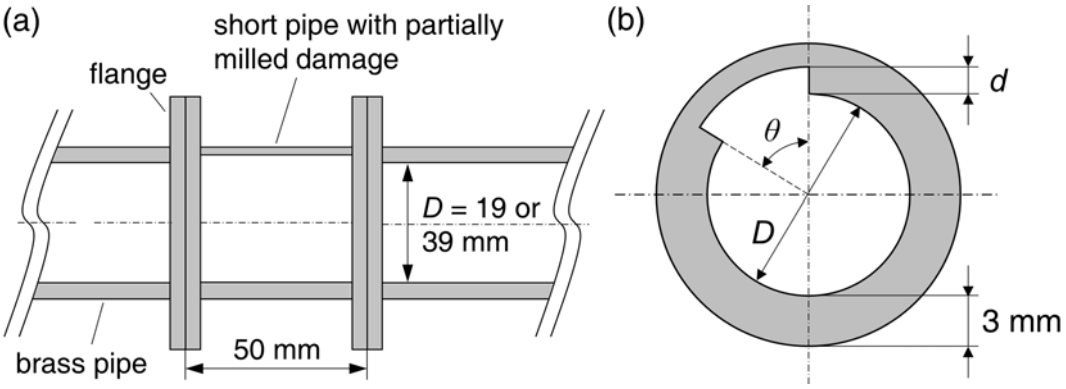

Figure 10. Illustration of the short pipe with partially milled damage. (a) Side view, (b) cross-section. (not to scale)

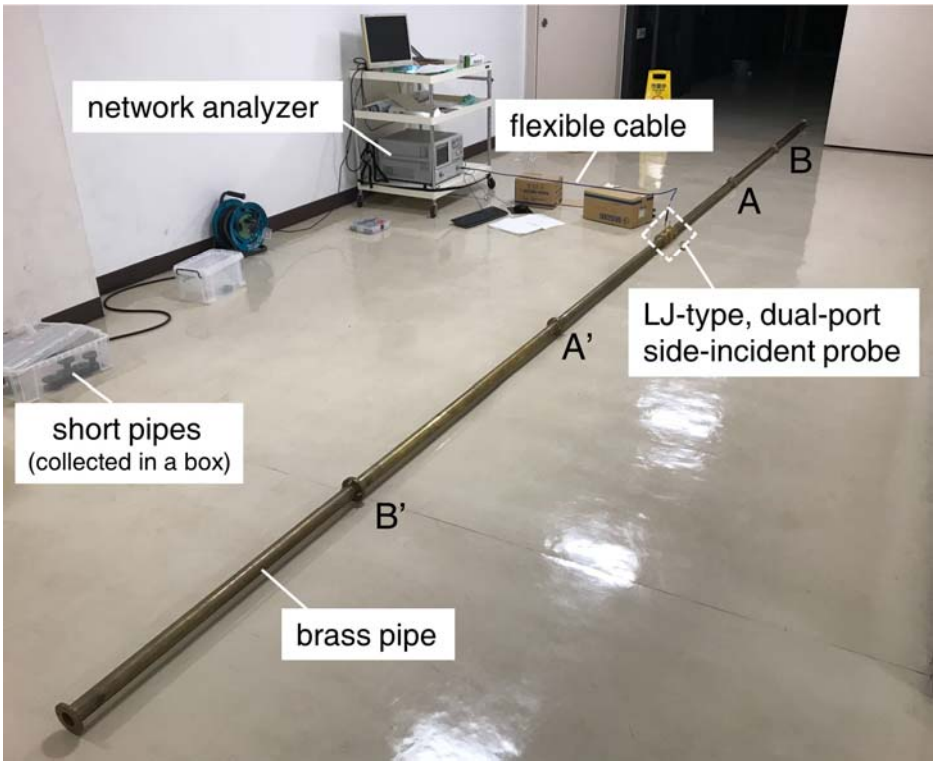

Figure 11. Photograph of the experimental setup.

Table 2. Dimensions of the short pipes used in the experiment.

No.	D (mm)	d (mm)	θ (deg.)
1	19.0	0	0
2	19.0	0.5	90
3	19.0	0.5	180
4	39.0	0	0
5	39.0	2	45
6	39.0	2	90

Figure 12 shows the 19 mm and 39 mm LJ-type, side-incident probes. The probes were fabricated by inserting semi-rigid cables (Anritsu Corporation, K118) into a brass pipe, on which two through-wall grooves were fabricated for cable insertion. The cables were manually bent into certain curvature radii using the self-designed benders made of resin by 3D printing, and fixed to the pipe using an adhesive conductive epoxy (MG Chemicals, 8331). A connector (Anritsu Corporation Anritsu, K101F-R) was attached to the end of each cable for connection. Regarding the 19 mm side-incident probe shown in figure 12 (a), the dimensional parameters of the fabricated probe were r_C = 8 mm, l_E = 3 mm, and l_S = 7 mm, which were slightly different from the simulation results in Section 2.2. The change in probe dimensions was mainly due to the difficulty in bending the cable into a smaller curvature radius. The interval between the two ports was 84 mm, and the total length of the probe was 180 mm. However, the simulation result for the fabricated probe was comparable with the optimal result in 2.2.2 and possessed a similar transmission characteristic to that shown in figure 5. The 39 mm LJ-type side-incident probe consisted of two single-port, side-incident probes assembled face-to-face as shown in figure 12 (b). This fabrication process made it easier to control the position of the cable inside the pipe and the alignment of the two face-to-face situated cables. In the experiments, the working frequency spans for the 19 mm and 39 mm side-incident probes were 20.6–25.4 GHz and 8.8–11.6 GHz, respectively.

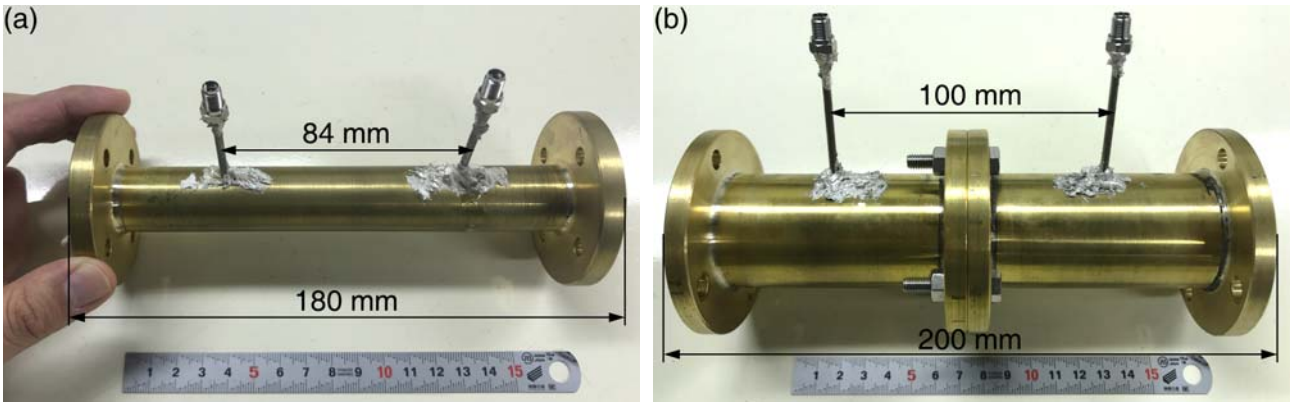

Figure 12. (a) 19 mm and (b) 39 mm LJ-type, side-incident probes.

The measurement was implemented in the frequency domain as a spectrum of the reflection coefficients (scattering parameters, S11). A total of 3,201 uniformly spaced points were sampled over

the working frequency span of each side-incident probe. The measured frequency domain reflection signals were subsequently converted into a time domain using the inverse fast Fourier transform with a Kaiser window function (shape factor was 6). According to the principle of inverse Fourier transform, the time-domain resolution of the converted signal is inversely proportional to the frequency span, while the time range is inversely proportional to the frequency-domain sampling interval. Therefore, when the frequency span is certain, the sampling rate in the frequency domain (3201 in this study) should be carefully chosen, to make sure the time range is large enough and the reflection from the pipe end is observable in the time-domain signal. Furthermore, we have not found any solid correlation between the frequency-domain sampling interval and the detectability of the proposed method. A signal-processing method [18,19] was also employed to compensate for the dispersion of microwaves during propagation and to locate flaws. The dispersion of microwaves was compensated by shifting the phase from a certain propagation distance to obtain a pulse, as given by the equation below:

$$\varphi(f) = 2L_C \cdot [\frac{1}{\lambda_P} - \frac{1}{\lambda}] \cdot 2\pi, \quad (2)$$

where φ denotes the shifted phase, f is the frequency, λ and λ_P refer to the wavelengths in free space and in a pipe, respectively. The coefficient 2 accounts for the roundtrip of microwave propagation. Since TM_{01} mode microwaves were dominant and mainly evaluated in the experiment, the parameter λ_P can be determined by the following equation:

$$\lambda_P = \frac{1}{\sqrt{(\frac{f}{c})^2 - (\frac{u_{01}}{\pi D})^2}}, \quad (3)$$

where c is the speed of light in a vacuum, D is the inner pipe diameter, and u_{01} is the first root of the Bessel function of the first kind, J_0. This process was conducted for a series of Lc (e.g., 0 to 5 m in this study). The position of the flaw was predicted by calculating the time-of-flight of the reflection without dispersion and obtaining the peak values for the distance range of the pipe length. A flow diagram depicting the signal-processing method is displayed in figure 13.

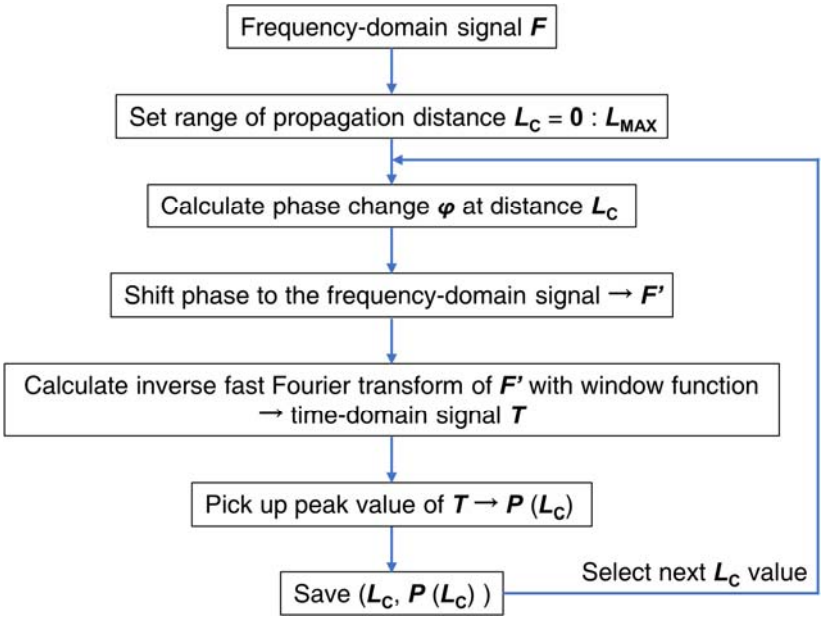

Figure 13. Flow diagram of the signal-processing method.

3.2 Results and discussion

Figures 14 and 15 present the processed reflection signals of 19 mm pipe and probe when ports L and R were used, respectively. When port L was adopted and the left pipe was under inspection (figure 14), the two types of in-pipe damage (short pipes 2 and 3) were detected at points A' and B' in the left pipe, whereas no obvious reflection signal from the in-pipe damage was observed when the in-pipe damage was deployed at points A and B in the right pipe. The large reflection appearing at 4 m corresponded to the left pipe end, whereas no noticeable reflection appeared at 4.5 m (right pipe end). Conversely, when port R was connected and the right pipe was inspected (figure 15), the reflections from the in-pipe damage situated at points A and B were discernible, whereas the in-pipe damage at points A' and B' was undetectable. The large reflection at 4 m was from the right pipe end, whereas no distinct reflection peak was observed at 4.5 m (left pipe end). Some small and dispersed reflections are observed between 1.5 m and 3 m in figures 14 and 15 that could have resulted from the spurious modes generated by the probe, such as the TE_{21} and TM_{11} modes. Moreover, the amplitudes of the reflection peaks in figure 14 (port L) are smaller than those in figure 15 (port R). The difference in reflection amplitude between the two ports could be attributed to the fabrication error when bending the cables. As the curvature radius r_C was merely 8 mm, and the bending process was performed manually, some deformations in the cross-section of the cables were inevitable. Nevertheless, comparing the amplitudes of the reflections from the in-pipe damage with those from the noises in figure 14 (a) and 15 (b), the results of the two ports show a similar signal-to-noise ratio and nearly consistent detection sensitivities. Therefore, a directional pipe inspection was realized by utilizing the proposed LJ-type, dual-port side-incident probe.

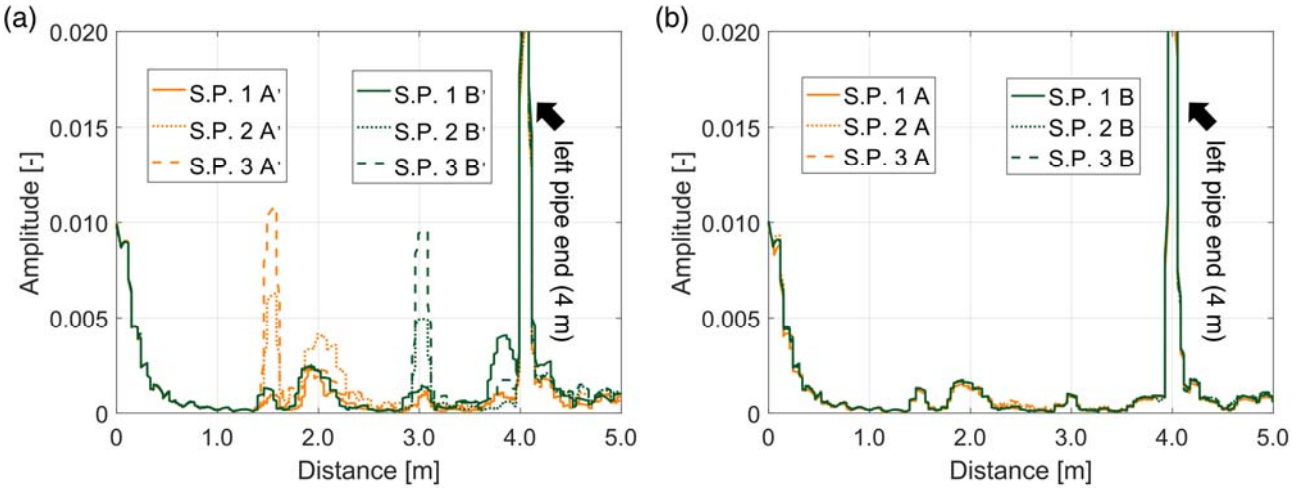

Figure 14. Refection signals from the in-pipe damage deployed at (a) points A' and B' and (b) points A and B when D =19 mm and port L of the probe was used. The left pipe was 4 m in length and the right pipe was 4.5 m. (S.P. = short pipe)

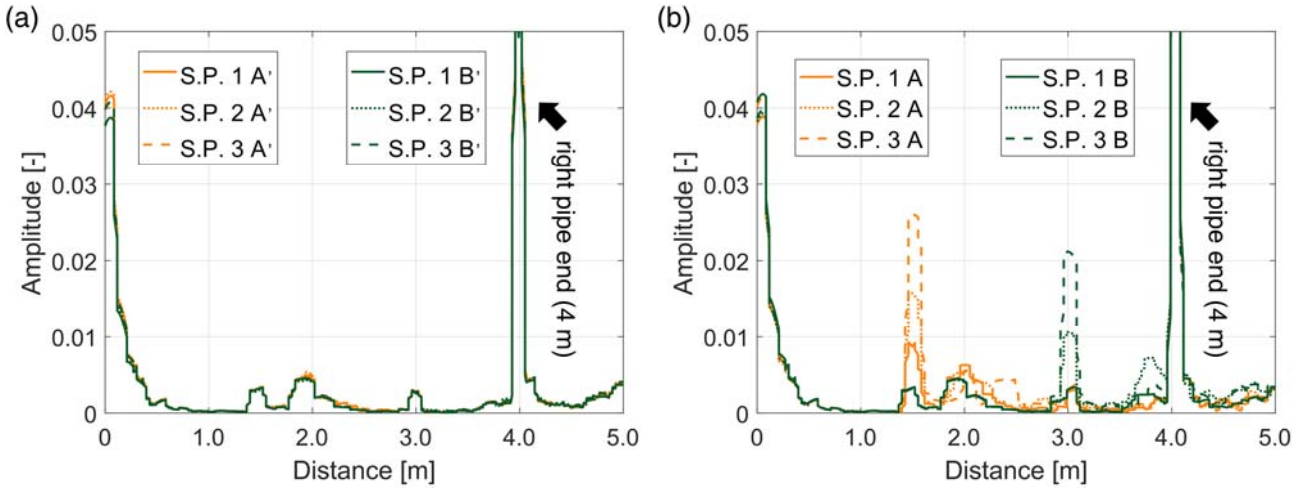

Figure 15. Refection signals from the in-pipe damage deployed at (a) points A' and B' and (b) points A and B when D =19 mm and port R of the probe was used. The right pipe was 4 m in length and the left pipe was 4.5 m. (S.P. = short pipe)

The experimental results for the 39 mm pipe and probe are shown in figures 16 and 17. Similar to the results of the 19 mm scenario, the 39 mm side-incident probe, which was developed based on the proportional relationship between the pipe diameter D and the dimensional parameters (r_C, l_E, and l_S), also showed a good detection directivity. The reflection signals of the two ports showed similar amplitudes, indicating that the two ports were almost identical. In summary, the experimental results presented in this section suggest that the proposed dual-port, side-incident probes can achieve directional pipe inspection with excellent directivity. Meanwhile, the applicability of this method to different inner pipe diameters has been confirmed.

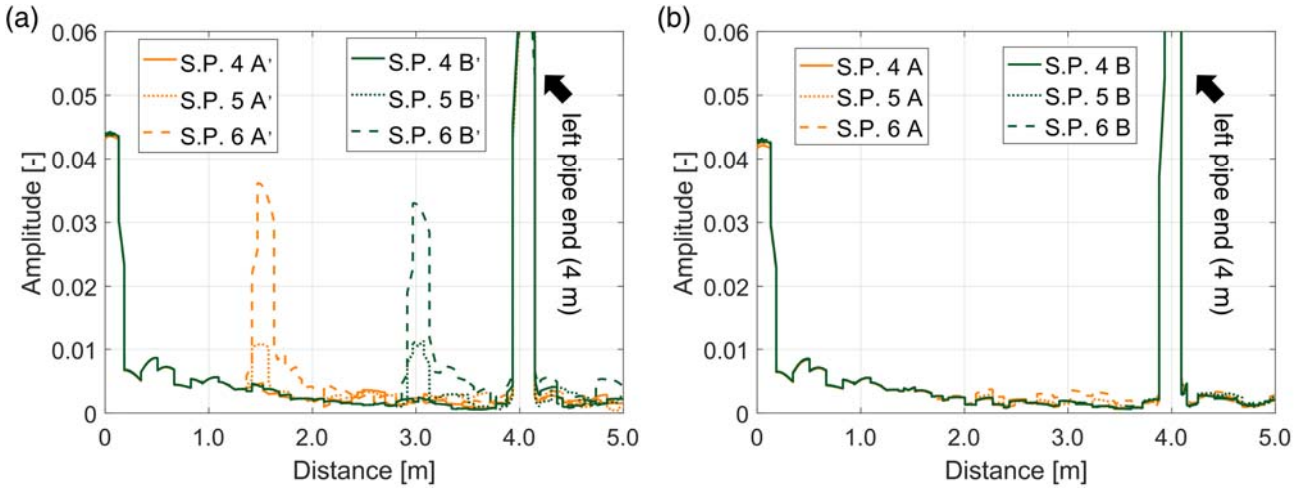

Figure 16. Refection signals from the in-pipe damage deployed at (a) points A' and B' and (b) points A and B when D =39 mm and port L of the probe was used. The left pipe was 4 m in length and the right pipe was 4.5 m. (S.P. = short pipe)

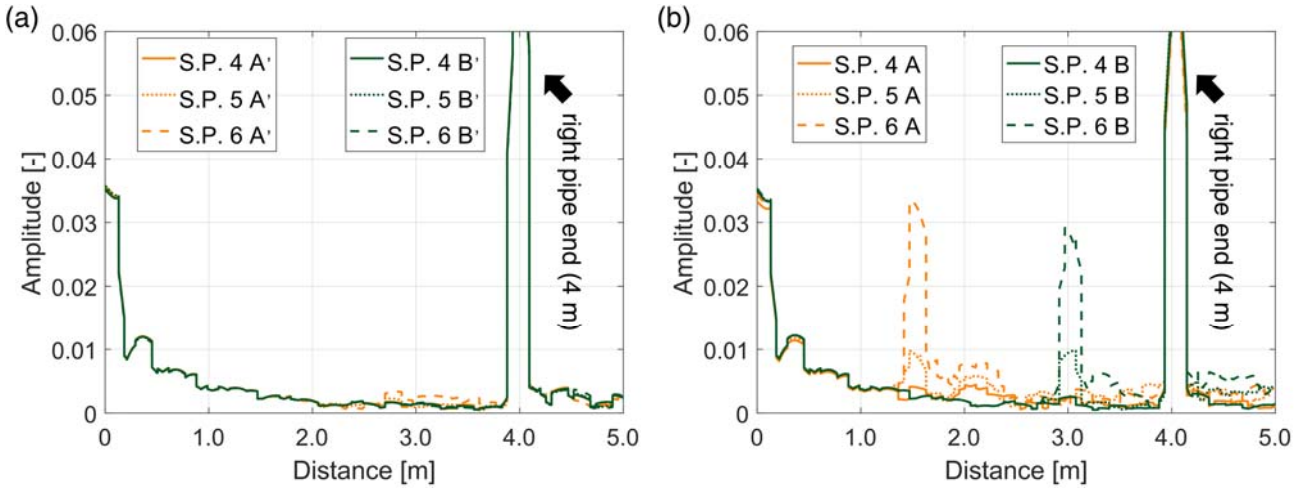

Figure 17. Refection signals from the in-pipe damage deployed at (a) points A' and B' and (b) points A and B when D =39 mm and port R of the probe was used. The right pipe was 4 m in length and the left pipe was 4.5 m. (S.P. = short pipe)

4. Conclusion

This study reported a dual-port, side-incident microwave probe for directional detection of in-pipe damage. Two types of probes (LJ and JL) were proposed based on the numerical simulations, and two LJ-type probes with different inner pipe diameters of 19 mm and 39 mm were fabricated and examined through an experiment. The simulation results suggested that an optimal selection of the three dimensional parameters (r_C, l_E, and l_S) of the probe could significantly improve the mode purity and transmission directivity of the probe. Besides, the optimized probe dimensions for one inner pipe diameter could also be applied to another diameter by proportionally changing the current probe dimensions with small adjustments. The results of the experimental verification showed that the in-pipe damage deployed on either side of each probe could be significantly detected and located using the corresponding port of the proposed dual-port probe. Adopting the side-incident method to other inner pipe diameters was verified to be feasible.

Acknowledgment

This study was partially supported by Grant-in-Aid for JSPS fellows (No. 18J20649). The authors would like to thank Mr. Takao Nagaya, who is affiliated with the School of Engineering, Tohoku University, for his assistance in the mechanical fabrication. The first author is grateful for the financial support provided by the China Scholarship Council (CSC).

Appendix

1. Supplementary information on the effect of r_C, l_S, and l_E

Figures 18–20 present the simulation results of the single-port probe and the effect of the dimensional parameters l_E, l_S, and r_C on the transmission characteristic of the probe. The reference values for l_E, l_S, and r_C were set to 4, 5, and 6 mm, respectively, for the comparison with the results of the other dimensional parameter combinations. The inner pipe diameter D was 19 mm, and the value of l_V was set to 10 mm. For simplicity, only the energy ratios of the TM_{01} and TM_{02} modes are exhibited in each figure.

Figure 18 shows the simulation results when r_C = 6, l_S = 5, and l_E = 3, 4 ,5 mm. Clearly, l_E affected

the transmission characteristic of the probe, as the energy ratio of the TM_{01} and TM_{02} modes transmitted to either left or right direction varied drastically. On the other hand, the effects of l_S and r_C were not as significant as that of l_E as shown in figures 19 and 20. Nevertheless, the difference in the energy ratio of each mode could still be discernibly observed for different l_S or r_C. Based on the above discussion, the correlation between the transmission characteristic of the probe and the dimensional parameters r_C, l_S, and l_E was proved.

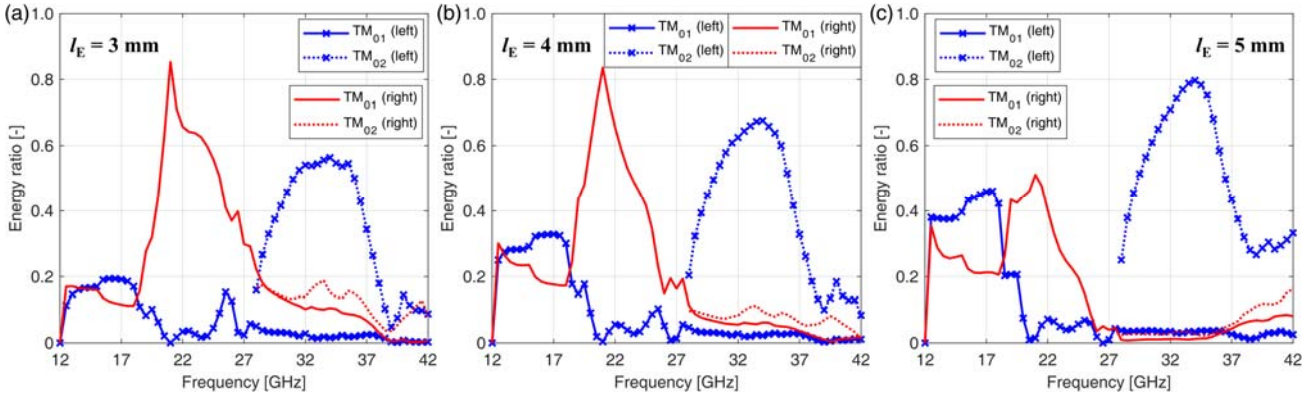

Figure 18. Simulation results of the single-port probe when r_C = 6 mm, l_S = 5 mm, and (a) l_E = 3 mm, (b) l_E = 4 mm, and (c) l_E = 5 mm.

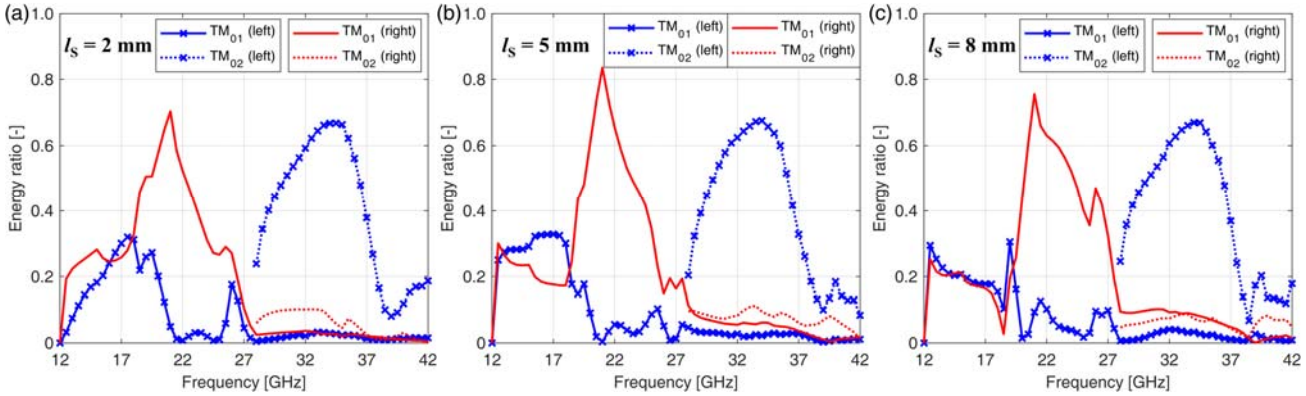

Figure 19. Simulation results of the single-port probe when r_C = 6 mm, l_E = 4 mm, and (a) l_S = 2 mm, (b) l_S = 5 mm, and (c) l_S = 8 mm.

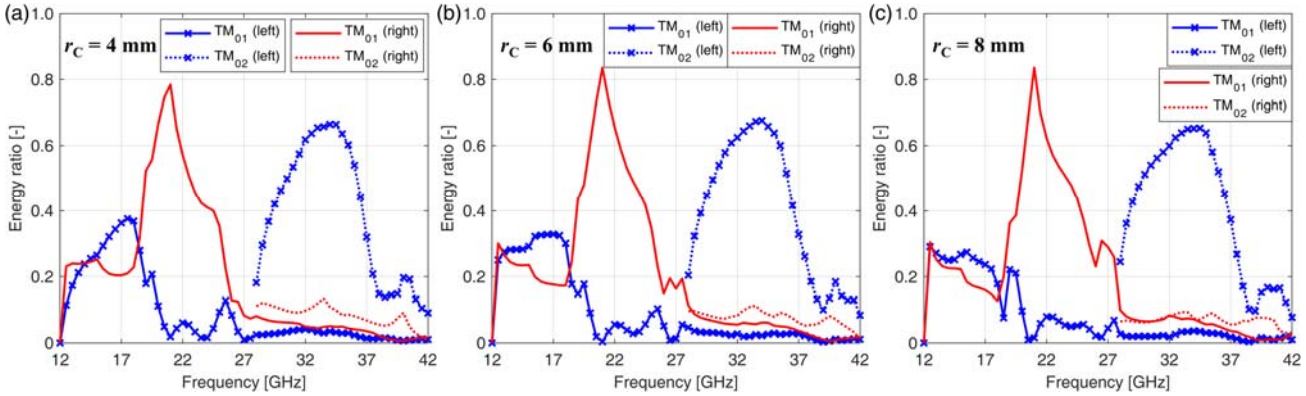

Figure 20. Simulation results of the single-port probe when l_S = 5 mm, l_E = 4 mm, and (a) r_C = 4 mm, (b) r_C = 6 mm, and (c) r_C = 8 mm.

2. Independence of l_V from the transmission characteristic of the probe

Figure 21 compares the simulation results of the single-port probe with the same r_C, l_E, and l_S but different l_V (10, 20, and 30 mm). The inner pipe diameter D was 19 mm. Interestingly, the results of each sub-figure show excellent consistency, demonstrating the irrelevance between l_V and the transmission characteristic of the probe.

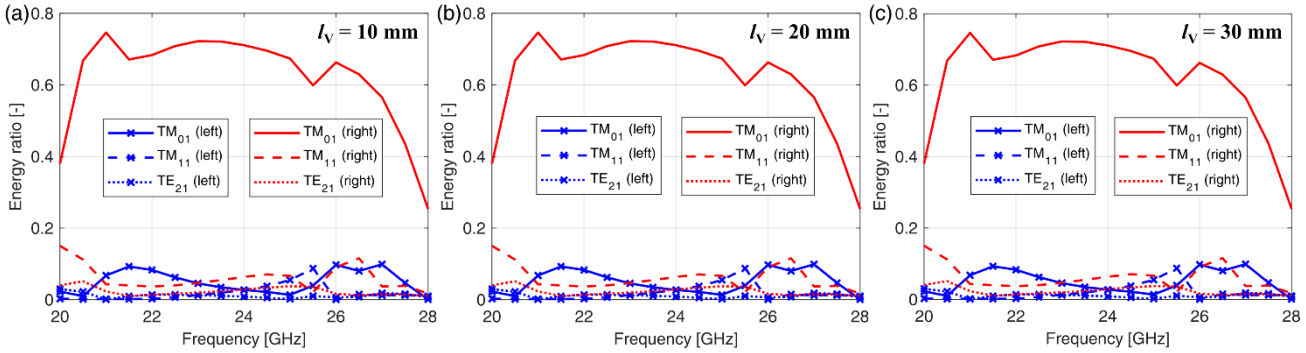

Figure 21. Simulation results of the single-port probe when r_C = 7 mm, l_E = 3 mm, l_S = 8 mm, and (a) l_V = 10 mm, (b) l_V = 20 mm, and (c) l_V = 30 mm.

3. Effect of the distance between two ports on the transmission characteristic of the probe

Figure 22 compares the simulation results of the LJ-type, dual-port probe with different distances between two ports. The inner pipe diameter D was 19 mm, and the TEM mode microwaves were excited at port L. The result shows that: the distance (interval) between the two ports did affect the transmission characteristic of the probe, and a longer interval seemingly did not mitigate the interference of the unused port or led to a better transmission characteristic.

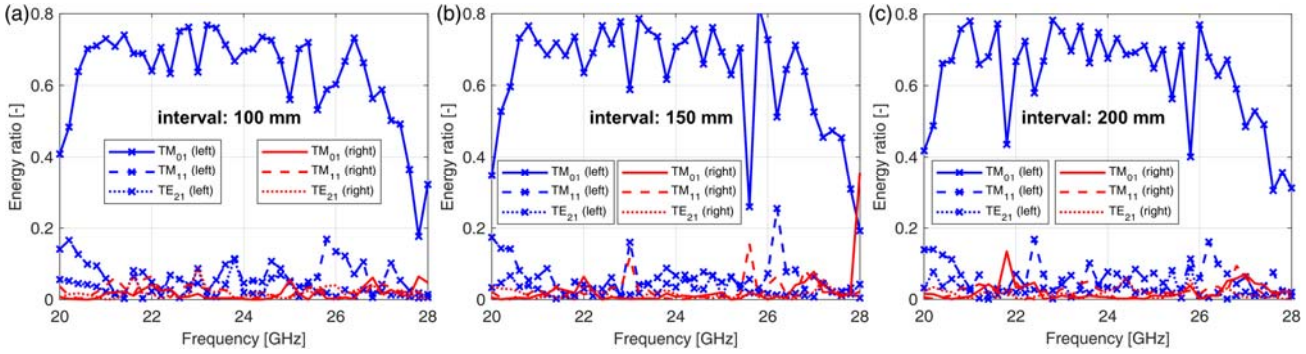

Figure 22. Simulation results of the LJ type, dual-port probe when r_C = 7 mm, l_E = 3 mm, l_S = 8 mm, and l_V = 10 mm and the distance (interval) between the two ports is (a) 100 mm, (b) 150 mm, and (c) 200 mm.

Reference

[1] Demma A, Cawley P, Lowe M, Roosenbrand AG, Pavlakovic B. The reflection of guided waves from notches in pipes: a guide for interpreting corrosion measurements. NDT & E International. 2004 Apr 1;37(3):167-80.

[2] Kim YY, Kwon YE. Review of magnetostrictive patch transducers and applications in ultrasonic nondestructive testing of waveguides. Ultrasonics. 2015 Sep 1;62:3-19.

[3] Huang H, Sakurai N, Takagi T, Uchimoto T. Design of an eddy-current array probe for crack sizing

in steam generator tubes. NDT & E International. 2003 Oct 1;36(7):515-22.
[4] Li Y, Yan B, Li W, Jing H, Chen Z, Li D. Pulse-modulation eddy current probes for imaging of external corrosion in nonmagnetic pipes. NDT & E International. 2017 Jun 1;88:51-8.
[5] Sugawara K, Hashizume H, Kitajima S. Development of NDT method using electromagnetic waves. JSAEM Stud. Appl. Electromagn. Mech. 2001;10:313-6.
[6] Shibata T, Hashizume H, Kitajima S, Ogura K. Experimental study on NDT method using electromagnetic waves. Journal of materials processing technology. 2005 Apr 10;161(1-2):348-52.
[7] Liu L, Ju Y. A high-efficiency nondestructive method for remote detection and quantitative evaluation of pipe wall thinning using microwaves. NDT & E International. 2011 Jan 1;44(1):106-10.
[8] Liu L, Ju Y, Chen M. Optimizing the frequency range of microwaves for high-resolution evaluation of wall thinning locations in a long-distance metal pipe. NDT & E International. 2013 Jul 1;57:52-7.
[9] Sasaki K, Katagiri T, Yusa N, Hashizume H. Demonstration of the Applicability of Nondestructive Microwave Testing to the Long-Range Inspection of Inner-Surface Cracks in Tubes. Materials Transactions. 2017 Apr 1;58(4):692-6.
[10] Katagiri T, Sasaki K, Song H, Yusa N, Hashizume H. Proposal of a TEM to TE 01 mode converter for a microwave nondestructive inspection of axial flaws appearing on the inner surface of a pipe with an arbitrary diameter. International Journal of Applied Electromagnetics and Mechanics. 2019 Jan 1;59(4):1527-34.
[11] Chen G, Katagiri T, Song H, Yusa N, Hashizume H. Detection of cracks with arbitrary orientations in a metal pipe using linearly-polarized circular TE11 mode microwaves. NDT & E International. 2019 Jun 1:102125.
[12] Jones RE, Simonetti F, Lowe MJ, Bradley IP. Use of microwaves for the detection of water as a cause of corrosion under insulation. Journal of Nondestructive Evaluation. 2012 Mar 1;31(1):65-76.
[13] Sasaki K, Katagiri T, Yusa N, Hashizume H. Experimental verification of long-range microwave pipe inspection using straight pipes with lengths of 19–26.5 m. NDT & E International. 2018 Jun 1;96:47-57.
[14] Uoshita S, Sasaki K, Katagiri T, Yusa N, Hashizume H. Long-range inspection of a pipe with a bend using microwaves. International Journal of Applied Electromagnetics and Mechanics. 2019 Jan 1;59(4):1519-1526.
[15] Chen G, Katagiri T, Song H, Yusa N, Hashizume H. Investigation of the Effect of a Bend on Pipe Inspection Using Microwave NDT. NDT & E International. 2019 Dec 9:102208.
[16] SASAKI K, YUSA N, KATAGIRI T, HASHIZUME H. Long-Range Inspection of a Pipe Using a Microwave Emitted by a Probe Attached to the Pipe Wall. Journal of the Japan Society of Applied Electromagnetics and Mechanics. 2017;25(2):266-72. (In Japanese)
[17] Anritsu Company, Precision RF & Microwave Components, Catalog No. 11410–00236, 2011.
[18] Sakai Y, Yusa N, Hashizume H. Nondestructive evaluation of wall thinning inside a pipe using the reflection of microwaves with the aid of signal processing. Nondestructive Testing and Evaluation. 2012 Jun 1;27(2):171-84.
[19] Katagiri T, Sasaki K, Yusa N, Hashizume H. Development of long-range inspection using TE mode microwaves for detecting axial cracks. Transactions of the JSME. 2018;84(859):17-00375. (In Japanese)